Geophysical Journal International

Geophys. J. Int. (2010) **183,** 225–236 doi: 10.1111/j.1365-246X.2010.04726.x

Elastic moduli evolution and accompanying stress changes with increasing crack damage: implications for stress changes around fault zones and volcanoes during deformation

M. J. Heap,[1]* D. R. Faulkner,[2] P. G. Meredith[1] and S. Vinciguerra[3]

[1]*Rock & Ice Physics Laboratory, Department of Earth Sciences, University College London, Gower Street, London WC1E 6BT, UK. E-mail: m.heap@ucl.ac.uk*

[2]*Rock Deformation Laboratory, Department of Earth and Ocean Sciences, University of Liverpool, Brownlow Street, Liverpool* L69 3GP, *UK*

[3]*Istituto Nazionale di Geofisica e Vulcanologia, Sezione di Roma1, Via di Vigna Murata* 605, 00143 *Rome, Italy*

Accepted 2010 July 6. Received 2010 July 6; in original form 2010 March 22

SUMMARY

The elastic moduli of rock in areas susceptible to crack damage, such as within fault zones or volcanic edifices, can be subject to large modifications. Knowledge of how elastic moduli may vary in such situations is important for both the reliable modelling of volcano deformation and stability and for linear and non-linear elastic crack models for earthquake rupture. Furthermore, it has previously been shown that changes in elastic moduli can induce changes in the stress field surrounding faults. Here we report both uniaxial experimental measurements of changes in elastic moduli during increasing-amplitude cyclic stressing experiments on a range of different rock types (basalts, sandstones and granite) and the results of modelled stress modifications. The trend in elastic moduli evolution with increasing damage was remarkably similar for each rock type, with the exception of essentially crack-free intrusive basalt that exhibited very minor changes. In general, Young's modulus decreased by between 11 and 32 per cent and Poisson's ratio increased by between 72 and 600 per cent over the total sequence of loading cycles. These changes are attributed to an increasing level of anisotropic crack damage within the samples. Our results also show that acoustic emission (AE) output during any loading cycle only commenced when new crack damage was generated. This corresponded to the level of stress where AE ceased during the unloading portion of the previous cycle. Using the multilayer elastic model of Faulkner *et al*. we demonstrate that the damage-induced changes in elastic moduli also result in significant decreases in differential stress, increases in mean stress and rotation of the applied greatest principal stress relative to the orientation of the mechanical layering. The similar trend in the evolution of the elastic moduli of all the rocks tested suggests that stress modification in the damage zone of faults might take the same form, regardless of the lithology through which the fault runs. These observations are discussed in terms of their applicability to both fault zones and deformation at volcanoes.

Key words: Fracture and flow; Earthquake dynamics; Volcano seismology; Acoustic properties; Dynamics and mechanics of faulting; Volcanic hazards and risks.

1 INTRODUCTION

Elastic moduli are the key parameters that relate stress to strain. They determine subyield differential stress states, the propagation velocity of elastic (seismic) waves and can be used to relate strain measurements to *in situ* stresses within the Earth's crust. Crack damage caused by stress perturbations and locally high stresses, such as those present within fault zones (e.g. Sibson 1986) or volcanic edifices (e.g. Allard *et al.* 2006), can produce large changes in the elastic moduli of rock (e.g. Gudmundsson 2004; Faulkner *et al.* 2006; Heap & Faulkner 2008; Heap *et al.* 2009a).

For faults, it is now well established that fracture density decreases as a function of distance away from the fault core (Anders & Wiltschko 1994; Vermilye & Scholz 1998; Wilson *et al.* 2003; Mitchell & Faulkner 2009). The quantification of the changes in elastic moduli as a result of increasing crack damage is a key input into universal-scaling laws that describe linear and non-linear elastic (or post-yield) crack models for earthquake rupture (Gudmundsson 2004) as well as for stress distribution and fault

*Now at: Section for Mineralogy, Petrology and Geochemistry, Department of Earth and Environmental Sciences, Ludwig-Maximilians-University Munich, Theresienstr. 41, 80333 München, Germany.

displacement models within and surrounding fault zones (Faulkner *et al.* 2006).

In volcanic areas, a significant hazard is posed by shallow-level edifice deformation, instability and susceptibility to flank collapse (Siebert 1992; McGuire 1996). Assessing the processes involved in flank destabilization and flank movement requires precise knowledge of the changes of elastic moduli under increasing stress (e.g. Walter *et al.* 2005). Knowledge of changes in elastic moduli for volcanic rock is also important for (1) the reliable modelling of the ground deformation at volcano edifices (most consider an isotropic elastic half-space to analyse surface deformation, e.g. see Dzurisin 2006), hindered by the presence of mechanical layering (see Manconi *et al.* 2007) and (2) the calibration of damage mechanics criteria for the weakening of rocks forming volcanic edifices and the development of appropriate time-to-failure laws needs a robust knowledge of mechanical properties of the representative rocks and their modification under stress (Voight 1989; Kilburn 2003; Kilburn & Sammonds 2005). Furthermore, it is very common for edifices to contain large faults, for example, the Pernicana Fault at Mt Etna. It is therefore possible that stresses surrounding such faults will also be modified (as per Faulkner *et al.* 2006) due to the increasing level of crack damage as the fault is approached.

However, the bulk of experimental studies on the evolution of static elastic moduli with increasing crack damage have been conducted on granites, generally of low porosity and low initial crack density (e.g. Alm *et al.* 1985; Martin & Chandler 1994; Eberhardt *et al.* 1999; Lau & Chandler 2004; Heap & Faulkner 2008) and the modelling of stress modifications due to such changes in elastic moduli is only reported for Westerly granite (WG; Faulkner *et al.* 2006).

The above-mentioned studies have shown that, at least for granites, increasing crack damage within a rock alters the static elastic moduli in granitic rocks significantly. However, large changes in static elastic moduli with respect to increasing crack damage have also been reported for an extrusive lava flow basalt containing a pre-existing network of interconnected microcracks of thermal cooling origin (Heap *et al.* 2009a) and for an oolitic iron ore (Wassermann *et al.* 2009). Similar changes in dynamic elastic moduli with respect to increasing cyclic damage have also been reported for a sandstone (Bagde & Petroš 2005). The modelled stress rotations reported for WG by Faulkner *et al.* (2006) are substantial and have important implications for fault zones mechanics.

It is now clear that additional rock types need to be investigated. Not only do fault zones traverse a wide range of lithologies, with different mechanical properties and porosities but due to the variability of the volcanics forming the lava pile at an edifice, reliable ground deformation modelling requires the knowledge of numerous representative lithologies, both extrusive and intrusive. Notwithstanding that large faults also traverse such lava piles. Furthermore, some volcanic edifices, for example, Mt Etna volcano, are underlain by a thick sedimentary substratum (Catalano *et al.* 2004) that can play a major role in flank instability (Borgia *et al.* 1992; Van Wyk De Vries & Borgia 1996).

Therefore, we report results from a study in which we measured the degradation of elastic moduli during increasing amplitude, cyclic-stressing experiments on both intrusive basalt (IB) and extrusive basalt (EB) and two sandstones. We then compare these data with equivalent measurements from experiments on a different basalt (Heap *et al.* 2009a) and a granite (Heap & Faulkner 2008). Acoustic emission (AE) output was recorded continuously during the cyclic stressing as a proxy measure of crack damage evolution. The experimental data for all of the above lithologies were then modelled to investigate the changes in stress state associated with changing elastic moduli during deformation and are discussed in terms of their application to fault zones and volcano deformation.

2 EXPERIMENTAL MATERIALS AND METHODOLOGY

The rock types investigated in this study are (1) an EB from Stromboli volcano, Italy (SB), which contains pre-existing microcracks due to rapid thermal cooling and a weak (∼5 per cent) but clear ultrasonic wave anisotropy, interpreted as resulting from the active tectonics within the volcano (Vinciguerra *et al.* 2006); (2) a fresh, intrusive columnar basalt from Seljadur, Iceland (IB) which, due to its long cooling history, does not contain any visible pre-existing microcracks and therefore has a very low porosity (Vinciguerra *et al.* 2005); (3) a very high porosity, quartz-rich sandstone from Bentheim, Germany (BHS); (4) a high porosity, well-indurated, feldspathic sandstone from Darley Dale, northern England (DDS). The modal compositions and physical properties of each rock type are summarized in Table 1.

Samples of all the rocks tested were cored to a diameter of 25 mm and ground flat and parallel within ±0.02 mm to a nominal length of 75 mm. All experiments were performed in a servo-controlled, uniaxial loading frame in the Rock and Ice Physics Laboratory at University College London (Fig. 1) and were conducted at ambient temperature. Axial and radial strains were continuously monitored throughout each experiment using displacement transducers. The output of AE energy was also continuously recorded by a MISTRAS-2001 AE recording system via a broadband PZT piezoelectric AE transducer located inside the bottom loading anvil (Fig. 1; see also Heap *et al.* 2009a for full details of the experimental configuration).

In the first cycle during increasing-amplitude stress-cycling experiments, samples were loaded to a maximum stress of 20 MPa at a constant strain rate of 7.0×10^{-6} s^{-1} and then unloaded at the same rate to 8 MPa. In each subsequent cycle, the maximum stress was increased by 10 MPa and samples again unloaded to 8 MPa. Stress cycling was continued in this way until all samples eventually failed. The stress cycling and therefore elastic moduli determination, began at a stress of 20 MPa in order to avoid the concave portion at the start of the stress–strain curves, typically associated with crack closure.

Following the method of Heap & Faulkner (2008), each of the unloading portions of the stress–strain curves was fitted with a third-order polynomial in order to ascertain the extent of the linear elastic portion of each curve. The resultant equations were then differentiated and the slopes of the stress–strain curves determined over their entire lengths. The static elastic moduli were then calculated from the linear regions of the curves (i.e. those regions where moduli did not change).

Experimental results on these rocks from this study are also compared with data from two previous stress-cycling studies on an EB from Mt Etna, Italy (Heap *et al.* 2009a) and low porosity WG from Rhode Island, USA (Heap & Faulkner 2008). The modal compositions and physical properties of these two rock types are also included in Table 1.

3 MECHANICAL DATA

Representative stress–strain curves from increasing-amplitude, stress-cycling experiments on EB (fig. 2a from Heap *et al.* 2009a),

Table 1. The modal composition and relevant physical properties of each of the studied rocks.

Rock type	Modal composition	Porosity (per cent)	Grain size (μm)	Unconfined compressive strength (MPa)	References
Etna basalt (EB)	Microcrystalline groundmass (∼60 per cent) with phenocrysts of plagioclase (25 per cent), pyroxene (9 per cent) and olivine (4 per cent)	Connected porosity of 4.4 per cent. Total porosity of 4.8 per cent	Microcrystalline groundmass with large phenocrysts (200–2500)	140	Heap *et al*. (2009a)
Stromboli basalt (SB)	Microcrystalline groundmass (∼50 per cent) with phenocrysts of plagioclase (35 per cent), pyroxene (10 per cent) and olivine (5 per cent)	3.7 ± 0.26	Microcrystalline groundmass with large phenocrysts (200–2500)	100	This study
Icelandic basalt (IB)	Microcrystalline groundmass comprising microlites of olivine, plagioclase and pyroxene and some iron oxides	1.2 ± 0.19	Microcrystalline groundmass	360	Vinciguerra *et al*. (2005)
Bentheim sandstone (BHS)	95 per cent quartz, 3 per cent kaolinite and 2 per cent orthoclase feldspar	23.4 ± 1.2	50–500	40	Heap *et al*. (2009c)
Darley Dale sandstone (DDS)	69 per cent quartz, 26 per cent feldspar, 3 per cent clay and 2 per cent mica	13.3 ± 0.8	100–800	60	Heap *et al*. (2009b)
Westerly granite (WG)	28 per cent quartz, 36 per cent microcline, 31 per cent plagioclase, 5 per cent biotite	0.8 ± 0.12	750	200	Heap & Faulkner (2008)

SB (fig. 2b), IB (fig. 2c), BHS (fig. 2d), DDS (Fig. 2e) and WG (Fig. 2f; from Heap & Faulkner 2008) are given in Fig. 2. Our data show that each successive loading cycle produced a change in the stress–strain response of the rock. This change is observed for all of the rock types tested, although the changes are smaller for IB and WG than for the other rock types. Eventually the samples failed, generally by axial splitting, after multiple loading cycles. We observe that IB is significantly stronger than the other basalts; with a peak stress (σ_P) of approximately 360 MPa as against 140 MPa for EB and 100 MPa for SB. It is also stronger than WG (σ_P = 200 MPa). The sandstones are much weaker, with DDS and BHS having peak stresses of 60 and 40 MPa, respectively (Fig. 2). The open circles on the volumetric strain curves in Fig. 1 mark the onset of dilatancy during each stress cycle, commonly denoted as C′ (e.g. see Wong *et al.* 1997). We note that, for all rock types tested, the stress at which C′ occurs remains essentially constant over all cycles, even though the strain at which C′ occurs increases with increasing cycle number.

Values of Young's modulus and Poisson's ratio, calculated from the data of Fig. 2, are plotted against cycle number for each of the six rock types in Fig. 3. The pattern of the evolution of the two static elastic moduli with increasing cycle number was very similar for each of the rock types tested, with the notable exception of IB. In general, Young's modulus decreased by between 11 and 32 per cent and Poisson's ratio increased dramatically by between 70 and 600 per cent; becoming close to 0.5 at failure (Fig. 3 and Table 2). The proportional decrease in Young's modulus was highest for the SB and EB and lowest for the porous sandstones (DDS and BHS) and the granite (WG). Whilst the relative changes in Poisson's ratio varied considerably between the different rock types, as noted above, the absolute changes were over a relatively narrow range from 0.20 to 0.36 (Table 2). Although the Young's modulus of IB initially decreased in a similar manner to that of the other rock types, the Poisson's ratio remained essentially constant throughout (Fig. 3c).

The AE output from each of the experiments (with the exception of the experiment on WG, where AE was not recorded) are shown plotted against stress and time in Fig. 4. The solid circles on the curves indicate the point at which AE output commenced on each loading cycle. In general, the observed pattern of AE activity was very similar for all five rock types. During most cycles, the output of AE recommenced on any loading cycle at the same level of stress that it ceased during the unloading portion of the previous cycle, as previously reported for EB by Heap *et al.* 2009a. We also note that the amount of AE energy emitted during the final loading cycle, where microcracks link and coalesce to produce macroscopic failure of the sample, was much greater (in general, by at least two orders of magnitude) than for any of the previous cycles.

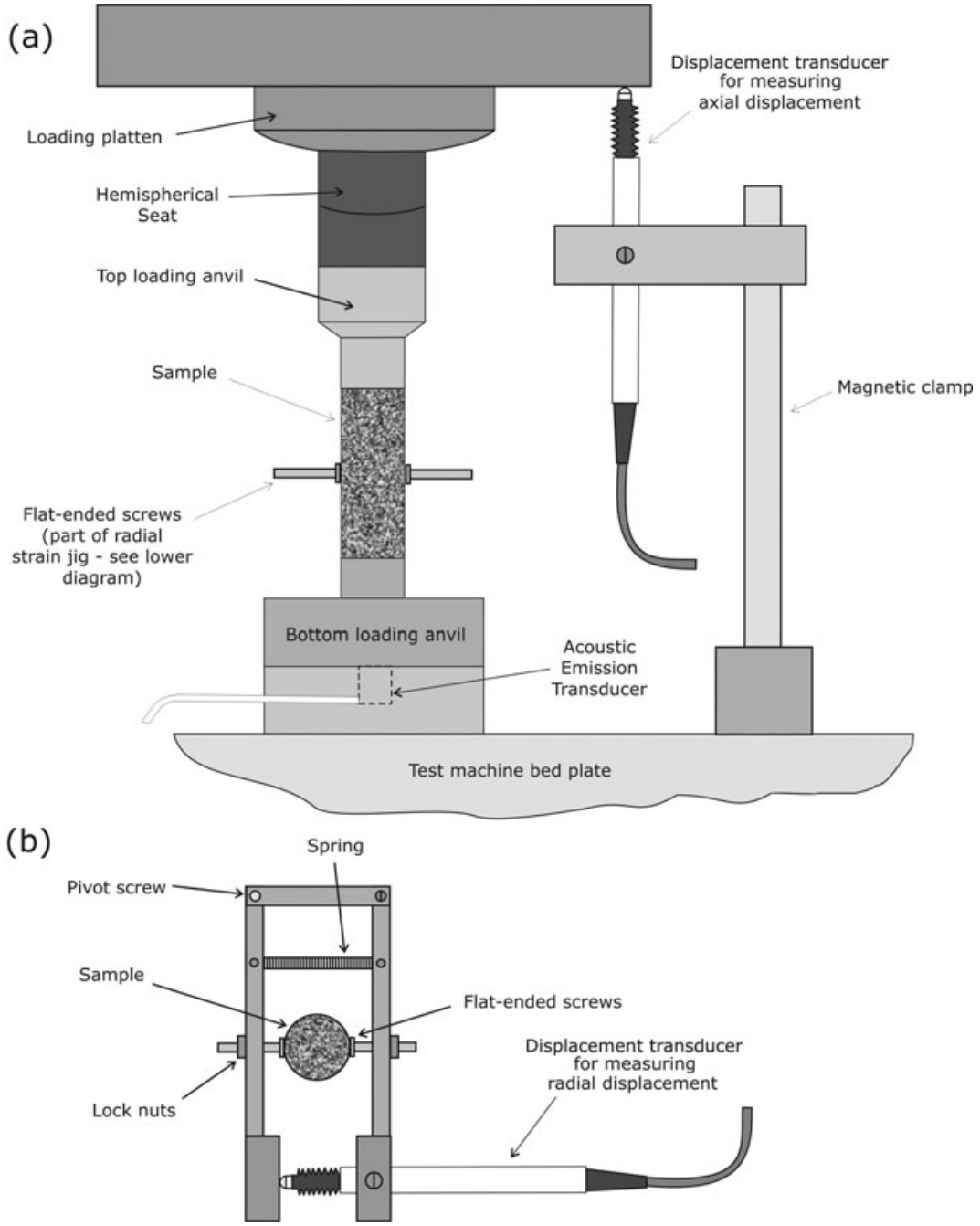

Figure 1. Schematic diagram of the experimental arrangement: (a) elevation showing the loading components and the positions of the axial displacement and AE transducer; (b) plan view showing the arrangement measurement of radial displacement.

4 STRESS MODIFICATION DUE TO ELASTIC MODULI CHANGES

Stress rotation is a well-documented process both for fault zones such as the San Andreas Fault (Zoback *et al.* 1987) and volcanic edifices such as Kilauea (Gillard *et al.* 1996) and Mt Etna (Barberi *et al.* 2004). Accumulating crack damage can be spatially heterogeneous. Thus, the magnitude and orientation of remotely applied stresses can be modified locally by local changes in elastic moduli as a result of accumulating crack damage (Faulkner *et al.* 2006).

In a general sense, the experiments were designed simply to highlight that deformation within highly stressed rock (such as within a volcanic edifice or a fault zone) which results in an increase in crack damage, will also result in significant changes in elastic moduli; key parameters in most mechanical modelling. More specifically, the experiments were designed to impart increments of crack damage in each sequential loading cycle, while measuring the concomitant changes in elastic moduli. In this way, each sequential loading cycle essentially simulates the changes in crack density (and therefore in elastic moduli) of the rocks in each layer of our multilayer model as we go from intact (undamaged)

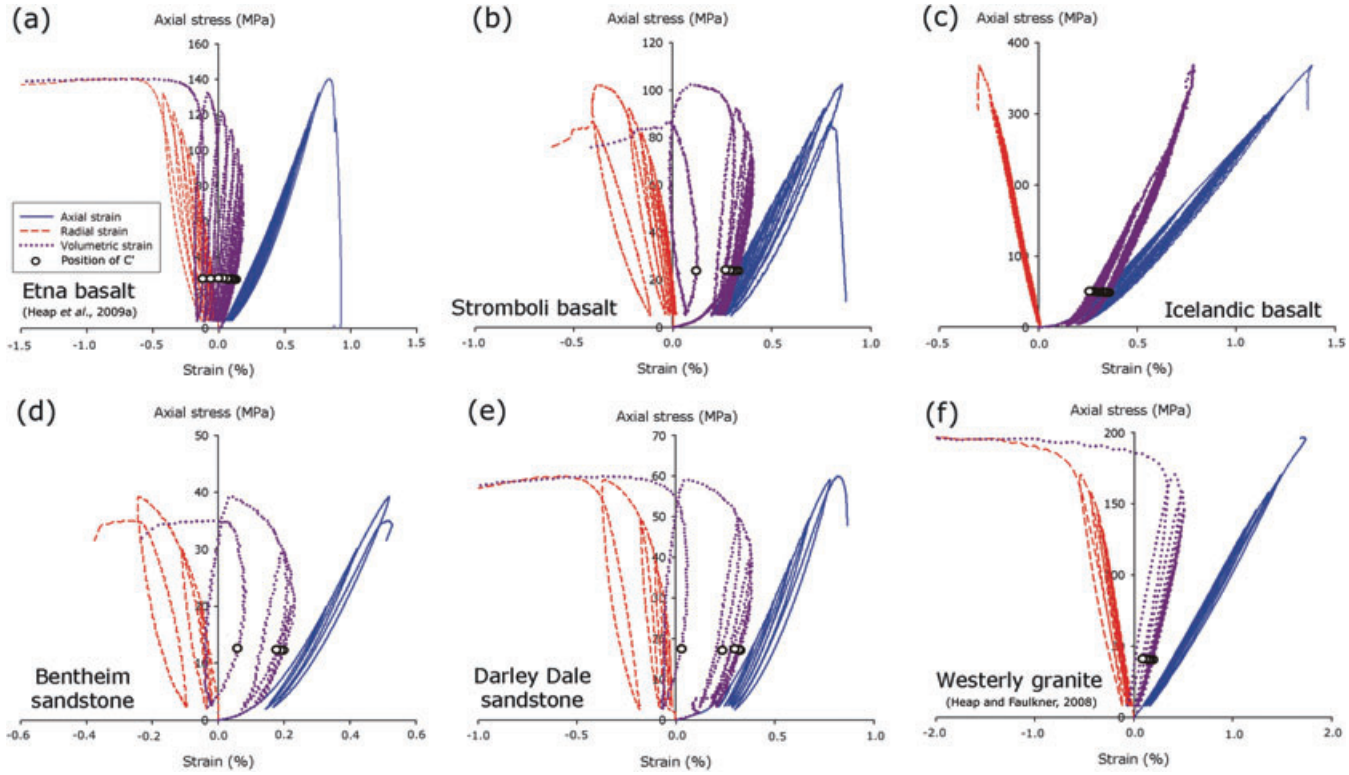

Figure 2. Representative stress–strain curves for (a) EB, (b) SB, (c) IB, (d) BHS, (e) DDS and (f) WG subjected to increasing-amplitude stress cycling. Data for EB is from Heap *et al*. (2009a), and data for WG is from Heap & Faulkner (2008). The open circles denote the onset of dilatancy (C′) for each stress cycle.

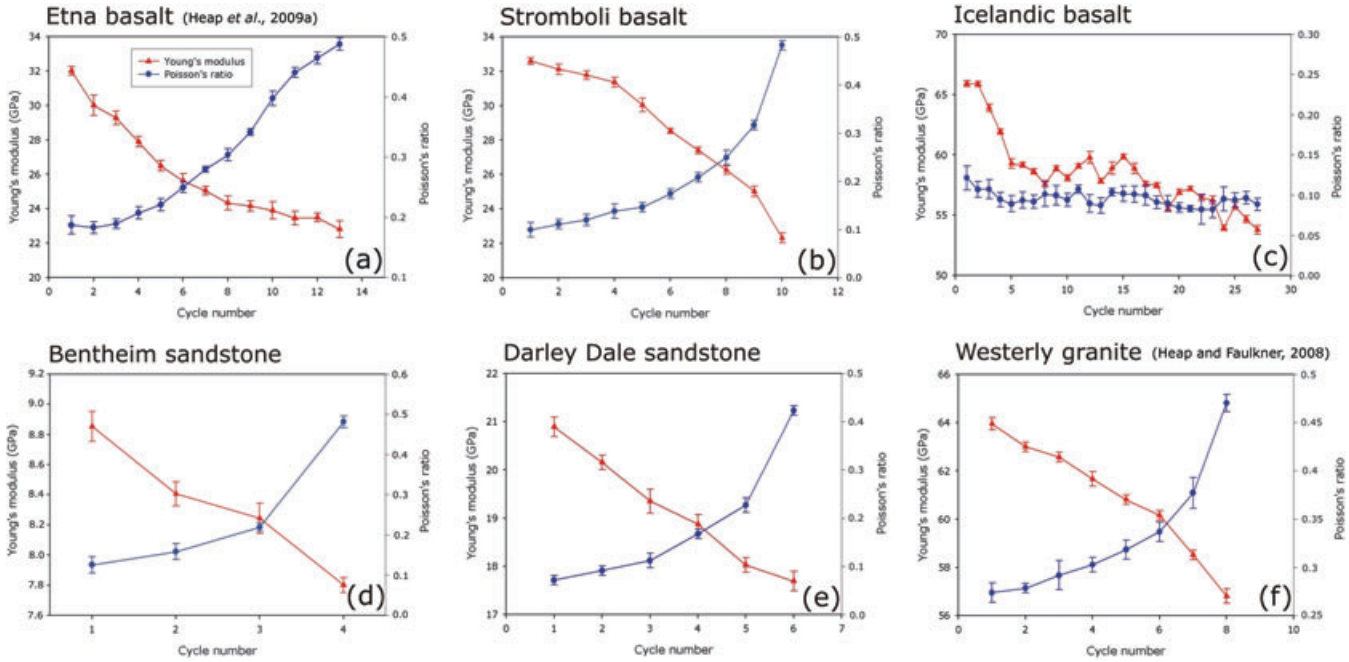

Figure 3. Evolution of static elastic moduli with increasing cycle number from increasing-amplitude stress-cycling experiments on (a) EB, (b) SB, (c) IB, (d) BHS, (e) DDS and (f) WG. Data for EB is from Heap *et al*. (2009a) and data for WG is from Heap & Faulkner (2008).

country rock to highly damaged rock as we approach the fault core.

Faulkner *et al*. (2006) modelled such stress modifications in the damage zone around a fault that was unfavourably oriented with respect to the remotely applied stress field. We take the same approach below in modelling our experimental data to illustrate the effect that the observed changes in elastic moduli might induce in the *in situ* local state of stress experienced by the six rock types under scenarios relevant to deformation in fault zones and volcanic edifices.

Table 2. Summary of the influence of increasing-amplitude stress-cycling on the static elastic moduli of all the rock types tested in this study and those from Heap & Faulkner (2008) and Heap *et al*. (2009a). The values presented represent total changes in elastic moduli during the course of complete experiments. The table also includes dynamic elastic moduli changes measured during triaxial deformation of Darley Dale sandstone at a confining pressure of 150 MPa, from Ayling *et al*. (1995).

Rock type	Decrease in Young's modulus (per cent)	Increase in Poisson's ratio (per cent)	Increase in Poisson's ratio
Etna basalt (Heap *et al.* 2009a)	29	250	0.29
Stromboli basalt	32	485	0.38
Icelandic basalt	19	Negligible	Negligible
Bentheim sandstone	12	380	0.36
Darley Dale sandstone	15	600	0.35
Westerly granite (Heap & Faulkner 2008)	11	72	0.20
Darley Dale sandstone (confining pressure = 150 MPa) (Ayling *et al.* 1995)	28	55	0.11

4.1 Description of the model

The model used to assess the changes in stress state resulting from changes in elastic moduli is a modification of that developed by Casey (1980). Multiple, parallel layers of varying elastic moduli (Young's modulus and Poisson's ratio) are envisaged (Fig. 5), with the moduli ranging from those corresponding to intact rock, to those corresponding to the damage state immediately prior to failure.

For faulting, the parallel layers of varying elastic moduli are taken to represent the changing level of crack damage in the damage zone surrounding a fault core, with the crack damage envisaged to form prior to the application of the remotely applied stresses imposed in the model. For a volcanic edifice, it is taken to represent the layering of a number of alternating pyroclastic and extrusive lava flow deposits, each with different physical and elastic moduli, a setting very common for basaltic volcanoes (Manconi *et al.* 2007). Furthermore, the accumulation of damage within a volcanic edifice over time, due to the coupling between its growth, major episodes of dyke intrusion, active tectonics and gravitational instability, is likely to produce regions where the elastic moduli alter the stress state prior to possible collapse and failure (Tibaldi 2001; Tibaldi & Groppelli 2002; Acocella & Neri 2003).

If x defines the direction parallel and y the direction normal to the elastic layering (Fig. 5), then the boundary conditions of the model are given by

$$\left.\begin{aligned} \sigma_{yy} &= \sigma'_{y} \\ \sigma_{xy} &= \sigma'_{xy} \\ \varepsilon_{xx} &= \varepsilon'_{xx} \end{aligned}\right\}, \tag{1}$$

where the primes denote the stresses or strains in the adjacent layer with different elastic properties. Hence the shear and normal stresses parallel and perpendicular to the elastic layering are fixed. From a consideration of mechanical continuity (force balance) and assuming plane strain deformation, the stresses are related to the strains in the following way:

$$\begin{Bmatrix} \sigma_{xx} \\ \sigma_{yy} \\ \sigma_{xy} \end{Bmatrix} = \begin{Bmatrix} d_{11} & d_{12} & d_{13} \\ d_{21} & d_{22} & d_{23} \\ d_{31} & d_{32} & d_{33} \end{Bmatrix} \begin{Bmatrix} \varepsilon_{xx} \\ \varepsilon_{yy} \\ \varepsilon_{xy} \end{Bmatrix}. \tag{2}$$

If isotropic elasticity is assumed within each layer, then the deformation matrix $\{D\}$ is given by

$$\{D\} = \frac{E(1-\nu)}{(1+\nu)(1-2\nu)} \times \begin{Bmatrix} 1 & \nu/(1-\nu) & 0 \\ \nu/(1-\nu) & 1 & 0 \\ 0 & 0 & (1-2\nu)/(1-\nu) \end{Bmatrix}, \tag{3}$$

where E is Young's modulus and ν is Poisson's ratio (Casey 1980; Zienkiewicz & Taylor 2005).

Since the remotely applied principal stresses are prescribed, this allows the normal and shear tractions relative to the layering to be calculated. The strains can be calculated from eq. (2). Using the boundary conditions in eq. (1), σ_{xx} can then be computed sequentially for each adjacent layer with their different elastic moduli. The orientation and magnitude of the principal stresses within each layer can then be determined from the standard equations for the transformation of stresses (Jaeger *et al.* 2007, chapter 2).

For the analysis presented here, the values used for the remotely applied stresses were $\sigma_1 = 60$ MPa, $\sigma_3 = 30$ MPa, with an angle θ of 75° between σ_1 and the layers (this would equate to a misorientated fault). The stress state used in the modelling ($\sigma_1 = 60$ MPa and $\sigma_3 = 30$ MPa) was chosen explicitly to be well below both the fracture and frictional strengths of all the rock types tested, so that an elastic analysis is appropriate. The appropriate failure mechanism is Mohr–Coulomb faulting and frictional sliding since the value of σ_3 is much lower than the minimum required to allow localized compactive deformation to occur in even the weakest and most porous rock tested (Bentheim sandstone). Clearly this puts a limit on the modelling which would not be appropriate at much higher differential stresses.

As we want to apply our results to cracked rock at non-zero (but shallow depths) we have used a non-zero value for σ_3 in the model despite having performed uniaxial tests (where $\sigma_3 = 0$). This is clearly an approximation, but we contend that the resultant trends in the moduli will be the same, and the magnitude of the changes similar, at shallow depths. Indeed, even at a confining pressure of 150 MPa, five times higher than that used in our model, the data of Ayling *et al*. (1995) show the same trend for DDS (see Table 2), although their elastic moduli changes are significantly reduced at this pressure. The increase in Poisson's ratio at a confining pressure of 150 MPa is only 55 per cent, compared to an increase of 600 per cent under uniaxial conditions. However, we contend that

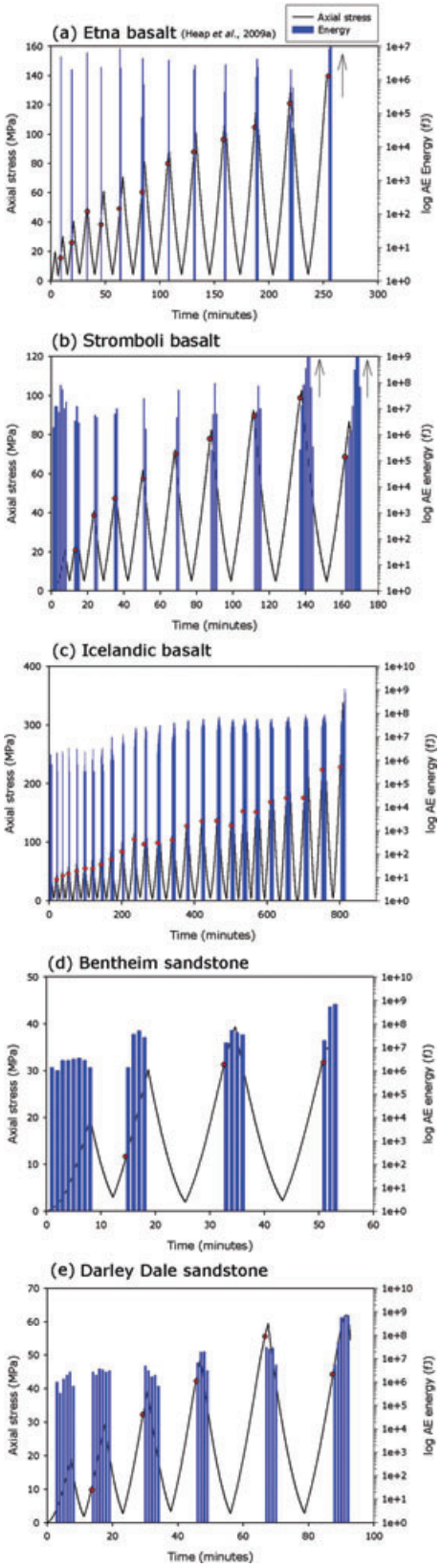

Figure 4. Output of AE energy in femto Joules for (a) EB, (b) SB, (c) IB, (d) BHS and (e) DDS as a function of stress and time, from increasing-amplitude, stress-cycling experiments. Solid circles indicate the points at which AE output recommenced on each loading cycle. Arrows indicate the position where AE energy increased beyond the scale displayed. Data for EB is from Heap *et al*. (2009a). Data is binned in minute intervals.

even a 55 per cent increase will result in stress modification, justified by a significant stress modification for WG under uniaxial conditions (Fig. 7), measured by Heap & Faulkner (2008); Poisson's ratio for WG only increased by 72 per cent. Nevertheless, future work will concentrate on performing similar cyclic loading experiments under triaxial stress at elevated σ_3.

In the experiments, all the rocks tested failed after a different number of stress cycles and hence, in order to allow comparison between them, we have normalized the changes in elastic moduli from 'intact' to 'failure' (Fig. 6). Our multilayer analysis presented here is a simplified one since, it assumes elastic heterogeneity between each layer, it assumed elastic isotropy within each layer. Previous observations (e.g. Anders & Wiltschko 1994; Vermilye & Scholz 1998; Wilson *et al.* 2003; Mitchell & Faulkner 2009) have demonstrated that the crack density increases in fault damage zones from a minimum background level in the country rock to a maximum as the fault core is approached, and this leads to elastic heterogeneity across the zone. In addition, earlier experimental studies have shown that an elastic anisotropy develops during deformation (e.g. Ayling *et al.* 1995; Stanchits *et al.* 2003). Anisotropy development will be especially prevalent under the uniaxial conditions of our experiments, where there microcracks are preferentially orientated in the axial direction so that transverse elastic moduli are likely to exhibit a greater change with deformation. Therefore, since our elastic moduli are measured in an axial orientation we have measured the stiffest values and they can therefore be considered to represent the minimum change that might be expected. Hence, although assuming elastic isotropy, we consider that our analysis uses the most appropriate values of Young's modulus and Poisson's ratio.

Elastic isotropy within each layer can be a good approximation for some geological settings, such as in lava flows where crack damage is induced by slow cooling and is commonly isotropic (e.g. Vinciguerra *et al.* 2005). However, as mentioned above, the nature of crack damage in many geological settings, produced by tectonic stresses, will be inherently anisotropic. Healy (2008) has modified the model of Casey (1980) so that it may be used to predict stress changes for the cases of transversely isotropy and monoclinic elastic symmetry. Nevertheless, the modelling presented here provides a first-order approximation of the possible stress modifications and a comparison of the relative changes for a range of important rock types.

4.2 Model results

One of the key parameters for the modification of stress within our model of damaged layers is the obliquity of the applied stress to the plane of the mechanical layering. If the maximum principal stress is oriented orthogonal to the layering, there will be no modification of the stress state (Fig. 5a), whereas, if it is oblique to the layering then the stress state can be altered significantly (Fig. 5b). In Fig. 5(b), it can be seen that the remote shear and normal stresses are fixed in accordance with one of the boundary conditions of the model described in the previous section. However, if the rock has experienced local stresses closer to the failure stress, then the changes in the elastic moduli will progressively promote an increase in mean stress, a reduction in differential stress and rotation of the principal stress relative to the layering in the rock (labelled 'rotated 2θ' in Fig. 5a).

Fig. 7 shows how the differential stress, the mean stress and θ (the angle between σ_1 and the mechanical layering) vary as a function of changes in the elastic moduli over the range from that of intact

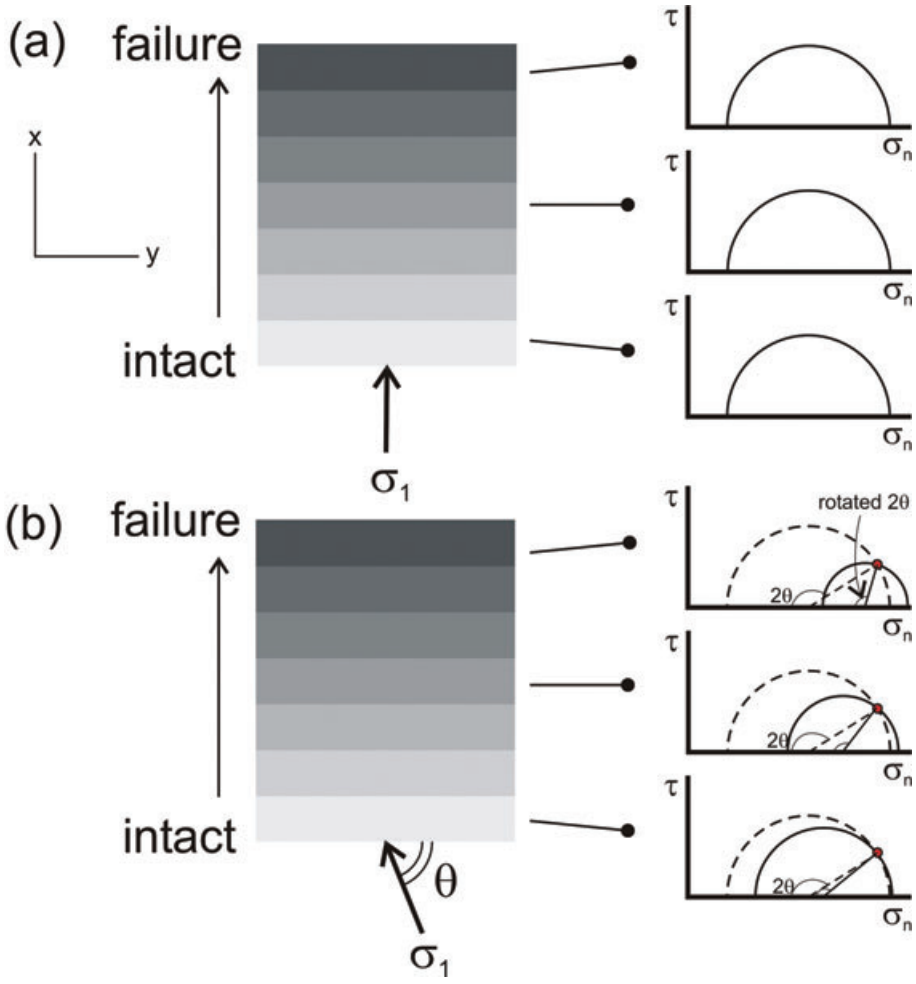

Figure 5. Schematic diagram illustrating how the orientation of principal stresses relative to the elastic layering will affect stress modification. (a) Where the principal stress is oriented normal to the layering, no stress changes will occur. (b) Where obliquity between the principal stress and layering occurs, large stress modification can occur, as illustrated by the solid Mohr circles.

rock to that of rock approaching failure. The change in stress state is considerably more dependent on the change in Poisson's ratio than the change in Young's modulus. Consequently, the stress changes are not large for IB, where there is little change in Poisson's ratio during stress cycling. However, the results are remarkably similar for all the other rock types. The changes are characterized by significant decreases in differential stress, increases in mean stress and rotation of the applied greatest principal stress relative to the orientation of the mechanical layering. However, such changes do not occur linearly with increasing damage level, so it should be pointed out that, while the changes in differential stress occur steadily with increasing damage, the mean stress and θ change much more rapidly above some apparent critical damage threshold (Fig. 7).

One feature of the model is that the stress can rotate past 45°. This corresponds to a minimum in the differential stress and as further stress rotation occurs, then the differential stress starts to increase. This case can be seen for BHS, EB and SB in Fig. 7. The general result of an increase in mean stress and decrease in differential stress means that the stress state migrates away from failure. We emphasize that, as the normal stress and shear stress remain fixed on planes parallel to the fault (a boundary condition for our model), failure may only be achieved by an increase in differential stress, or an increase in pore fluid pressure. However, the stress modifications do allow pore fluid weakening to occur without promoting tensile hydrofracture before fault slip if the fault is unfavourably orientated.

5 DISCUSSION

5.1 Micromechanical interpretation

Following previous studies (Eberhardt *et al.* 1999; Heap & Faulkner 2008; Heap *et al.* 2009a), we attribute the changes in sample stiffness during cyclic stressing that lead to the observed reductions in Young's modulus and increase on Poisson's ratio to an increasing level of anisotropic crack damage within the samples; either the extension of favourably oriented, pre-existing cracks, the propagation of new, axial cracks, or some combination of both. During each cycle in which samples are loaded to a successively higher stress an additional increment of crack damage is imparted to the sample, as evidenced by the output of AE. This leads to increasing amounts of irrecoverable strain on each cycle and was observed for all of the rock samples tested. The large increases in Poisson's ratio are likely to be due to the preferential formation and growth of axial cracks during deformation (Heap & Faulkner 2008; Heap *et al.* 2009a). Previous experimental studies have also shown that, generally for crystalline rocks, the level of microcrack damage influences static elastic moduli in the same manner as reported in this study (Alm

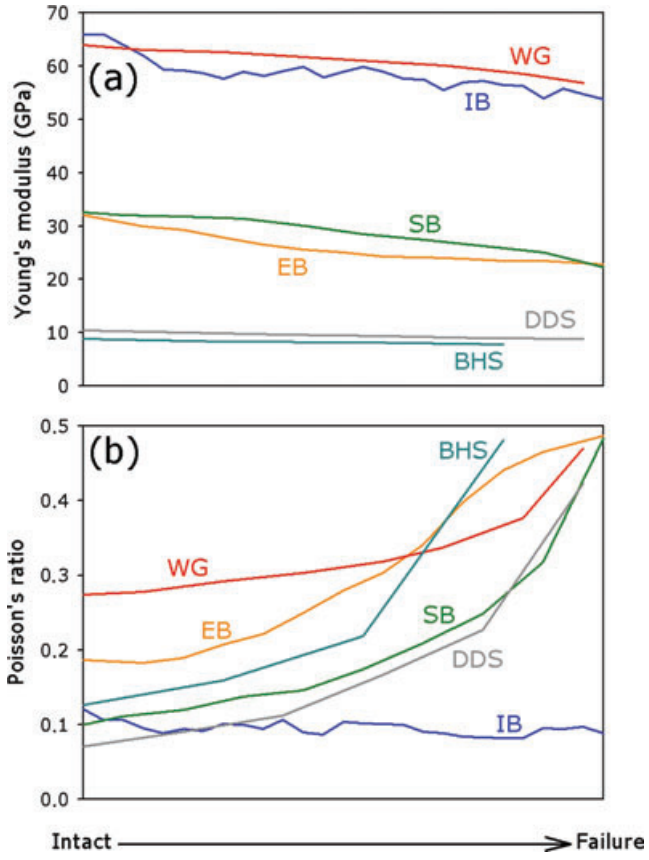

Figure 6. Synoptic diagram showing experimentally measured changes in elastic moduli normalized between 'intact' (indicating the moduli of the undeformed rock prior on the first loading cycle) and 'failure' (indicating the moduli immediately prior to failure on the final loading cycle).

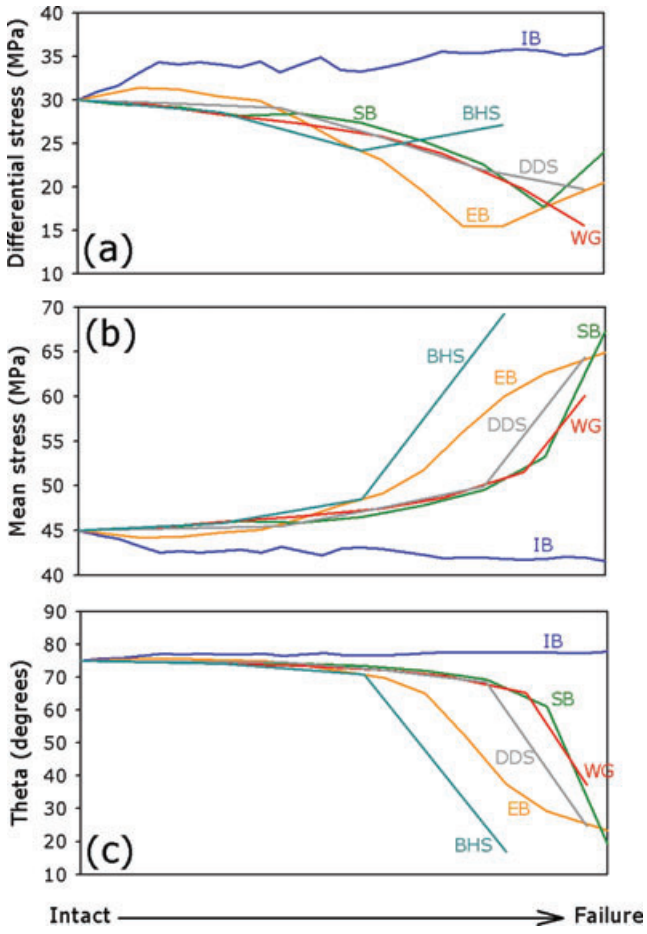

Figure 7. Modelled changes in the differential stress, mean stress and angle between the greatest principal stress and the elastic layering as a function of change in elastic moduli from the intact state to the failure state.

et al. 1985; Martin & Chandler 1994; Eberhardt *et al.* 1999; Lau & Chandler 2004).

However, the evolution of elastic moduli during cyclic stressing of IB was observed to be qualitatively different from all the other rock types tested. In this case, after an initial significant decrease, the Young's modulus decreased only marginally over the remaining loading cycles. Somewhat similarly, after a small initial decrease, the Poisson's ratio remained essentially constant during the remainder of the experiment. This difference in behaviour is attributed to the extremely homogeneous crystalline matrix and the absence of any visible pre-existing microcracks, which also results in IB having exceptionally high elastic wave velocities (Vinciguerra *et al.* 2005). The lack of microcracks therefore provides only scarce stress concentration points for the initiation of new cracks. Although AE output was observed during the cyclic loading of IB (Fig. 4c), the level is low in comparison to the high stresses applied to this very strong material. Furthermore, on failure, the sample shattered violently into coherent pieces with no evidence of any fault gouge, suggesting highly localized cracking. Such focussed deformation, concentrated very late in the deformation cycle, could explain the small increase in radial strain leading to an essentially constant Poisson's ratio.

Consistent with the observation noted by Heap *et al*. (2009a) from their study of cyclic stressing of EB, we also do not observe the classic interpretation of the Kaiser 'stress memory' effect (Kurita & Fujii 1979; Holcomb 1993; Li & Nordlund 1993; Lockner 1993; Lavrov 2003) in our cyclic stressing of SB, IB, BHS and DDS. In the classical interpretation, AE output should only be observed when the stress level in any loading cycle exceeds the maximum stress in any previous loading cycle. Rather, we observe a slight but significant variation from that behaviour, which we interpret in terms of time-dependent cracking. Crack growth is not instantaneous, so that during any loading cycle where the stress is continuously increasing, the propagation of new crack damage always lags somewhat behind the level theoretically associated with the instantaneous level of stress. This phenomenon can be observed in the data of Fig. 4, where AE output is seen to continue for some time after peak stress and into the unloading part of the cycle. Only when the AE ceases does the crack growth also cease. We therefore observe that AE output recommences during the next loading cycle at the same level of stress that it ceased during the unloading portion of the previous cycle. It is likely that if we used a much lower strain rate or if we held the stress at its peak level in each cycle (e.g. Wassermann *et al.* 2009) we would have observed a more classic manifestation of the Kaiser effect. However, in contrast, we deliberately used a rather high strain rate and did not hold samples at peak stress in order to minimize any effects of time-dependent, anelastic deformation. Even then, we were unable to eliminate it completely. That is why we record a small amount of AE for a short period during the unloading parts of the cycles. Consequently, we observe a variation on the classical Kaiser effect where AE on any cycle recommences at the stress at which it ceased on the unloading part of the previous cycle, rather than at the peak stress.

The onset of AE in any cycle marks the onset of new, dilatant cracking on that cycle, but is not commensurate with the onset of dilatancy; a relative increase in volume seen on the volumetric strain curves and marked by the open circles in Fig. 2. For each rock type tested, the stress at the onset of dilatancy remained essentially constant over all increasing-amplitude stress cycles. A constant onset of dilatancy was entirely as expected, since previously formed cracks that closed during unloading on the previous cycle re-open elastically to produce a dilatant volume increase during increased loading on the current cycle. Crack re-opening occurs at the same level of stress on every cycle irrespective of the level of damage. By contrast, the initiation of new, dilatant cracking (as marked by the onset of AE output) only commences when all the pre-existing crack damage has been fully opened. The new cracking therefore commences at a higher level of stress with each increasing cycle number and is marked by the solid circles on Fig. 4.

5.2 Applicability of the modelling approach

Healy (2008) has questioned the efficacy of applying elastic moduli determined from uniaxial compression experiments to modelling rock deformation in the crust. Rather, he argues that values for the elastic moduli computed from effective medium theory better represent those appropriate for stress states typical found at depth in the Earth's crust and compared his modelled data with measurements from triaxial deformation experiments. However, this comparison was made with data from experiments in which samples were monotonically loaded to failure in a single loading cycle. In this situation, the evolution of elastic moduli is a function not only of increasing crack damage but also of increasing differential stress (Brace *et al.* 1966; Schubnel *et al.* 2003; Katz & Reches 2004) and can result in masking of the changes in elastic moduli caused by the increase in crack damage. Heap & Faulkner (2008) showed that increasing axial stress and increasing level of crack damage induce opposite effects in the elastic moduli, at least for uniaxial loading. We posit that, during triaxial loading to failure in a single cycle (Brace *et al.* 1966; Schubnel *et al*. 2003; Katz & Reches 2004), the increase in differential stress is the dominant factor controlling the elastic moduli, rather than the increase in crack damage.

We would therefore argue that the evolution of elastic moduli as a function of increasing crack damage alone can only be determined from cyclic-stressing experiments, regardless of whether these are performed under a uniaxial or triaxial loading configuration. In cyclic tests, more crack damage may be imparted to the sample between stress cycles by raising the maximum value of differential stress from each cycle to the next (as was done in this study). The influence of differential stress may be removed by only considering the values for the elastic moduli at a constant value of differential stress. The contribution of differential stress to changes in the elastic moduli can also be determined by analysing the unloading portions of the stress–strain curves, where it is assumed that little or no further crack damage is accumulated. Hence any changes in elastic moduli will be solely due to the differential stress change. There may well be differences between the evolution of elastic moduli observed under uniaxial and triaxial stresses, but cyclic triaxial loading experiments would be required to determine these differences. Such a study is currently under way and will form the basis of a future companion paper. However, preliminary results indicate that very similar trends are observed under cyclic triaxial loading as those reported here for uniaxial loading.

5.3 Application to faults zone and volcanic deformation

The results presented here show how the elastic moduli change as crack damage is accumulated in rocks. For faults, it is now well established that fracture density decreases as a function of distance away from the fault core, as documented for highly indurated quartz sandstones (Vermilye & Scholz 1998), calcite and silica cemented sandstones (Anders & Wiltschko 1994; Wilson *et al.* 2003) and crystalline rocks, such as gneiss and granodiorites (Mitchell & Faulkner 2009). Hence, the parallel damage layers in our model can be taken to represent the damage zone of faults. The remarkably similar behaviour in the evolution of the elastic moduli of all the rocks tested with pre-existing crack damage (i.e. all the rocks except IB) suggests that stress modification in the damage zone of faults might take the same form almost regardless of the lithology through which the fault runs.

However, Shipton & Cowie (2001) have reported that the microfracture density surrounding faults developed in high porosity sandstones showed little variation with distance from the core. They attribute this to the different mechanics associated with the formation of deformation bands, that is, grain crushing caused by enhanced stress at grain contacts, which form without the production of easily quantifiable intra-granular microcracks. The microcracks that form are therefore compressive ('anticracks') and are not dilatant. Thus the stress field surrounding a fault in sandstone could actually therefore reduce as deformation progresses, explaining the lack of any microcrack signature related to the faulting. In contrast, our experimental data on high porosity BHS and DDS shows the same pattern of evolution of elastic moduli as that for the low porosity crystalline rock. This similarity suggests similar underlying micromechanical behaviour, that is, increased microcrack damage rather than grain crushing, perhaps because we 'forced' the stress to increase. It is clear that further investigation both in the field and in the laboratory is required to resolve the exact nature of the damage zone surrounding faults in different sandstones and of the evolution of the elastic moduli during the formation of deformation bands.

Volcanic edifices are commonly subject to repeated cycles of stress over time due to the combination of magma emplacement from deep reservoirs to shallow depths (Bonaccorso 1996; Allard *et al.* 2006; Palano *et al.* 2008; Puglisi *et al.* 2008; Carbone *et al.* 2009), dyke emplacement (McGuire *et al.* 1991) and superimposed tectonic stresses. Anisotropic deformation and an increase in the level of crack damage can therefore develop within the rocks that form the edifice and hence, changes to their elastic moduli (Heap *et al.* 2009a); a key observation for the reliable modelling of ground deformation. However, not only will the rock be likely to have different levels of damage, but composite volcanoes, made from multiple layers of material with different mechanical properties, will also have different starting elastic moduli and different responses to increasing stress. All of these variables should ideally be taken into account when performing ground displacement modelling (see also Manconi *et al.* 2007). This study also shows that, although the elastic response from the two EBs is similar, the difference between the extrusive and IB is substantial. Therefore, future studies should focus on as wide a range of volcanic material as possible, from very low porosity obsidian to scoriaceous basalts and andesites. The effect of exacerbated differences in elastic moduli between layers will also serve to increase the likelihood that an injected dyke will become arrested before reaching the surface (Gudmundsson 2005). Damage mechanics criterion for the weakening of rock prior to major fracturing events and the estimation of the critical strain for bulk failure also require precise knowledge of the elastic

moduli of the rock forming the edifice (Kilburn & Sammonds 2005). Moreover, for simplicity, such estimates of the critical strain for bulk failure generally assume that the crystal materials beneath the volcano are likely to share similar fracture mechanical properties. Furthermore, the degradation of elastic moduli that we observe under cyclic stressing implies that caution is needed when applying simple failure criteria (such as that of Hoek & Brown 1997) to studies of volcano flank stability (e.g. at Stromboli volcano; Apuani *et al.* 2005). This study has demonstrated that the cohesion, bulk strength and elastic moduli of lava flow units can be much lower than expected due to increased crack damage caused by stress cycling within the edifice.

Both concepts come together when considering the effect of changes in elastic moduli on the large faults that commonly traverse different layers within a volcanic edifice; such as the Pernicana Fault on Mt Etna volcano. Mt Etna is particularly important in this context since major faults not only propagate through sequences of basaltic and volcanic strata, but also through a thick sedimentary substratum (Catalano *et al.* 2004). Furthermore, the potential weakness of faults present in a volcanic edifice, exacerbated by damage-induced changes in the stress field, can promote fracturing and slip of unstable sectors and dyke injection (Heap *et al.* 2009a), thus increasing the potential for major episodes of slip or even flank collapse to occur at strato-volcanoes such at Mt Etna and Stromboli (Tibaldi 2001; Tibaldi & Groppelli 2002; Acocella & Neri 2003). Furthermore, the greatest principal stress will be orientated almost vertically and therefore at a high angle to the sub-horizontal layering in an edifice. The orientation of the stress will therefore be modified further because of the free surface; this modification will be especially true in shallow regions where there is surface topography. Finally, any rapid stress change and reorientation, as a result of dyke intrusion, can result in further rotation of the stress tensor controlling the main fault systems (Gillard *et al.* 1996; Barberi *et al.* 2004 and references therein).

6 CONCLUSIONS

(1) We have demonstrated that cyclic-stressing significantly alters the static elastic moduli of a range of different rock types. The trends in elastic moduli evolution with increasing crack damage were remarkably similar for all rock type tested, with the notable exception of IB. In general, Young's modulus decreased by between 11 and 32 per cent and Poisson's ratio increased by between 72 and 600 per cent over the total sequence of loading cycles. These changes are attributed to an increase in the level of crack damage with increasing stress on each cycle, evidenced by the output of AE energy.

(2) Our results also demonstrate that AE output can be used to discriminate between the onset of dilatancy and the onset of new, dilatant crack damage.

(3) Using the multiple-layer elastic model of Faulkner *et al*. (2006) we demonstrate that the damage-induced changes in elastic moduli also result in significant decreases in differential stress, increases in mean stress and rotation of the maximum principal stress relative to the orientation of the mechanical layering. The remarkably similar behaviour in the evolution of the elastic moduli of all the pre-damaged rocks tested illustrates that stress modification in the damage zone of faults might take the same form, regardless of the lithology through which the fault propagates. In volcanic environments, the potential weakness of faults present in an edifice, caused by the microcrack-induced changes in the stress field, could increase the likelihood of major episodes of slip or even flank collapse occurring at strato-volcanoes.

ACKNOWLEDGMENTS

We gratefully acknowledge John Bowles for the design and construction of the radial strain jig, Steve Boon for development and implementation of the load control system and Neil Hughes for help and support during experimentation. M. Heap was funded by NERC studentship NER/S/A2005/13553. S. Vinciguerra was funded by the FIRB-MIUR (Sviluppo Nuove Tecnologie per la Protezione e Difesa del Territorio dai Rischi Naturali). We would also like to thank J. Cowlyn, Y. Lavallée and P. Baud for helpful comments, R. Smith for help with the AE analysis and two anonymous reviewers and the editor, Jörg Renner, for constructive comments that improved the manuscript.

REFERENCES

Acocella, V. & Neri, M., 2003. What makes flank eruptions? The 2001 Etna eruption and its possible triggering mechanisms, *Bull. Volcanol.,* **65,** 517–529.

Allard, P., Behncke, B., D'Amico, S., Neri, M. & Cambino, S., 2006. Mount Etna 1993–2005: anatomy of an evolving eruptive cycle, *Earth-Sci. Rev.,* **78,** 85–114.

Alm, O., Jaktlund, L. & Shaoquan, K., 1985. The influence of microcrack density on the elastic and fracture mechanical properties of Stripa granite, *Phys. Earth planet. Inter.,* **40,** 161–179.

Anders, M.H. & Wiltschko, D.V., 1994. Microfracturing, paleostress and the growth of faults, *J. Struct. Geol.,* **16,** 795–815.

Apuani, T., Corazzato, C., Cancelli, A. & Tibaldi, A., 2005. Physical and mechanical properties of rock masses at Stromboli: a dataset for volcano instability evaluation, *Bull. Eng. Geol. Environ.,* **64,** 419–431.

Ayling, M.R., Meredith, P.G. & Murrell, S.A.F., 1995. Microcracking during triaxial deformation of porous rocks monitored by changes in rock physical properties, I. Elastic-wave propagation measurements on dry rocks, *Tectonophysics,* **245,** 205–221.

Bagde, M.N. & Petroš, V., 2005. Fatigue properties of intact sandstone samples subjected to dynamic uniaxial cyclical loading, *Int. J. Rock Mech. Min. Sci.,* **42,** 237–250.

Barberi, G., Cocina, O., Maiolino, V., Musumeci, C. & Privatera, E., 2004. Insight into Mt. Etna (Italy) kinematics during the 2002–2003 eruption as inferred from seismic stress and strain tensors, *Geophys. Res. Lett.,* **31,** L21614, doi:10.1029/2004GL020918.

Bonaccorso, A., 1996. Dynamic inversion of ground deformation data for modelling volcanic sources (Etna 1991–93), *Geophys. Res. Lett.,* **23**(5), 451–454.

Borgia, A., Ferrari, L. & Pasquare, G., 1992. Importance of gravitational spreading in the tectonic and volcanic evolution of Mount Etna, *Nature,* **357,** 231–235.

Brace, W.F., Paulding, B.W. & Scholz, C.H., 1966. Dilatancy in the Fracture of Crystalline Rocks, *J. geophys. Res.,* **71,** 3939–3953.

Carbone, D., D'Amico, S., Musumeci, C. & Greco, F., 2009. Comparison between the 1994–2006 seismic and gravity data from Mt. Etna: new insight into the long-term behavior of a complex volcano, *Earth planet. Sci. Lett.,* **279,** 282–292.

Casey, M., 1980. Mechanics of shear zones in isotropic dilatant materials, *J. Struct. Geol.,* **2,** 143–147.

Catalano, S., Torrisi, S. & Ferlito, C., 2004. The relationship between late quaternary deformation and volcanism of Mt. Etna (eastern Sicily): new evidence from the sedimentary substratum in the Catania region, *J. Volc. Geotherm. Res.,* **132,** 311–334.

Dzurisin, D., 2006. *Volcano Deformation,* Springer/Praxis, Chichester.

Eberhardt, E., Stead, D. & Stimpson, B., 1999. Quantifying progressive pre-peak brittle fracture damage in rock during uniaxial compression, *Int. J. Rock Mech. Min. Sci.,* **36,** 361–380.

Faulkner, D.R., Mitchell, T.M., Healy, D. & Heap, M.J., 2006. Slip on 'weak' faults by the rotation of regional stress in the fracture damage zone, *Nature,* **444,** 922–925.

Gillard, D., Rubin, A.M. & Okubo, P., 1996. Highly concentrated seismicity caused by deformation of Kilauea's deep magma system, *Nature,* **384,** 343–346.

Gudmundsson, A., 2004. Effects of Young's modulus on fault displacement, *C. R. Geodyn.,* **336,** 85–92.

Gudmundsson, A., 2005. The effects of layering and local stresses in composite volcanoes on dyke emplacement and volcanic hazards, *C. R. Geosci.,* **337,** 1216–1222.

Healy, D., 2008. Damage patterns, stress rotations and pore fluid pressures in strike-slip fault zones, *J. geophys. Res.,* **113,** B12407, doi:10.1029/2008JB005655.

Heap, M.J. & Faulkner, D.R., 2008. Quantifying the evolution of static elastic properties as crystalline rock approaches failure, *Int. J. Rock Mech. Min. Sci.,* **45,** 564–573.

Heap, M.J., Vinciguerra, S. & Meredith, P.G., 2009a. The evolution of elastic moduli with increasing crack damage during cyclic stressing of a basalt from Mt. Etna volcano, *Tectonophysics,* **471,** 153–160.

Heap, M.J., Baud, P., Meredith, P.G., Bell, A.F. and Main, I.G., 2009b. Time-dependent brittle creep in Darley Dale sandstone, *J. geophys. Res.,* **114,** B07203, doi:10.1029/2008JB006212.

Heap, M.J., Baud, P. & Meredith, P.G., 2009c. The influence of temperature on brittle creep in sandstones, *Geophys. Res. Lett.,* **36,** L19305, doi:10.1029/2009GL039373.

Hoek, E. & Brown, E.T., 1997. Practical estimates of rock mass strength, *Int. J. Rock Mech. Min. Sci.,* **34,** 1165–1186.

Holcomb, D.J., 1993. General theory of the Kaiser effect, *Int. J. Rock Mech. Min. Sci.,* **30,** 929–935.

Jaeger, J., Cook, N.G.W. & Zimmerman, R., 2007. *Fundamentals in Rock Mechanics,* 4th edn, Blackwell Publishing, London.

Katz, O. & Reches, Z., 2004. Microfracturing, damage and failure of brittle granites, *J. geophys. Res.,* **109,** B01206, doi:10.1029/2002JB001961.

Kilburn, C.R.J., 2003. Multiscale fracturing as a key to forecasting volcanic eruptions. *J. Volc. Geotherm. Res.,* **125,** 271–289.

Kilburn, C.R.J. & Sammonds, P.R., 2005. Maximum warning times for imminent volcanic eruptions, *Geophys. Res. Lett.,* **32,** L24313, doi:10.1029/2005GL024184.

Kurita, K. & Fujii, N., 1979. Stress memory of crystalline rocks in accousitc emission, *Geophys. Res. Lett.,* **6**(1), 9–12.

Lau, J.S.O. & Chandler, N.A., 2004. Innovative laboratory testing, *Int. J. Rock Mech. Min. Sci.,* **41,** 1427–1445.

Lavrov, A., 2003. The Kaiser effect in rocks: principals and stress estimation techniques, *Int. J. Rock Mech. Min. Sci.,* **40,** 151–171.

Li, C. & Nordlund, E., 1993. Experimental verification of the Kaiser effect in rocks, *Rock Mech. Rock Eng.,* **26,** 333–351.

Lockner, D., 1993. The role of acoustic emission in the study of rock fracture, *Int. J. Rock Mech. Min. Sci. Geomech. Abstr.,* **30,** 883–889.

Manconi, A., Walter, T.R. & Amelung, F., 2007. Effects of mechanical layering on volcano deformation, *Geophys. J. Int.,* **170,** 952–958.

Martin, C.D. & Chandler, N.A., 1994. The progressive fracture of Lac du Bonnet granite, *Int. J. Rock Mech. Min. Sci.,* **31,** 643–659.

McGuire, W.J., 1996. Volcano instability: a review of contemporary themes, *J. Geol. Soc. Lond.,* **110,** 1–23.

McGuire, W.J., Murray, J.B., Pullen, A.D. & Saunders, S.J., 1991. Ground deformation monitoring at Mt Etna: evidence for dyke emplacement and slope instability, *J. geol. Soc. Lond.,* **148,** 577–583.

Mitchell, T.M. & Faulkner, D.R., 2009. The nature and origin of off-fault damage surrounding strike-slip fault zones with a wide range of displacements: a field study from the Atacama fault system, northern Chile, *J. Struct. Geol.,* **31,** 802–816.

Palano, M., Puglisi, G. & Gresta, S., 2008. Ground deformation patterns at Mt. Etna from 1993 to 2000 from joint use of InSAR and GPS techniques, *J. Volc. Geotherm. Res.,* **169,** 99–120.

Puglisi, G., Bonforte, A., Ferretti, A., Guglielmino, F., Palano, M. & Prati, C., 2008. Dynamics of Mount Etna before, during and after the July–August 2001 eruption inferred from GPS and differential synthetic aperture radar interferometry data, *J. geophys. Res.,* **113,** B06405, doi:10.1029/2006JB004811.

Schubnel, A., Nishizawa, O., Masuda, K., Lei, X., Xue, Z. & Gueguen, Y., 2003. Velocity measurements and crack density determination during wet triaxial experiments on Oshima and Toki granites, *Pure appl. Geophys.,* **160,** 869–887.

Shipton, Z.K. & Cowie, P.A., 2001. Damage zone and slip-surface evolution over μm to km scales in high-porosity Navajo sandstone, Utah, *J. Struct. Geol.,* **23,** 1825–1844.

Sibson, R.H., 1986. Earthquakes and rock deformation in crustal fault zones, *Ann. Rev. Earth. planet Sci.,* **14,** 149–175.

Siebert, L., 1992. Threats from debris avalanches, *Nature,* **356,** 658–659.

Stanchits, S., Lockner, D. & Ponomarev, A., 2003. Anisotropic changes in *P*-wave velocity and attenuation during deformation and fluid infiltration of granite, *Bull. seism. Soc. Am.,* **93**(4), 1803–1822.

Tibaldi, A., 2001. Multiple sector collapses at stromboli volcano, Italy: how they work, *Bull. Volcanol.,* **63,** 112–125.

Tibaldi, A. & Groppelli, G., 2002. Volcano-tectonic activity along structures of the unstable NE flank of Mt. Etna (Italy) and their possible origin, *J. Volc. Geotherm. Res.,* **115,** 277–302.

Van Wyk De Vries, B. & Borgia, A., 1996. The role of basement in volcano deformation, *Geol. Soc. Lond.,* Special Publications, **110,** 95–110.

Vermilye, J.M. & Scholz, C.H., 1998. The process zone: a microstructural view of fault growth, *J. geophys. Res.,* **103**(B6), 12 223–12 237.

Vinciguerra, S., Trovato, C., Meredith, P.G. & Benson, P.M., 2005. Relating seismic velocities, thermal cracking and permeability in Mt. Etna and Iceland basalts, *Int. J. Rock Mech. Min. Sci.,* **42,** 900–910.

Vinciguerra, S., Lewis, O., Benson, P.M. & Meredith, P.G., 2006. Microstructural evidences of instability at Stromboli volcano: new insights from physical properties, *Geophysical Res. Abs.,* **8,** 01338.

Voight, B., 1989. A relation to describe rate-dependent material failure, *Science,* **243,** 200–203.

Walter, T.R., Acocella, V., Neri, M. & Amelung, F., 2005. Feedback processes between magmatic events and flank movement at Mount Etna (Italy) during the 2002–2003 eruption, *J. geophys. Res.,* **110,** B10205, doi:10.1029/2005JB003688.

Wassermann, J., Senfaute, G., Amitrano, D. & Homand, F., 2009. Evidence of dilatant and non-dilatant damage processes in oolitic iron ore: *P*-wave velocity and acoustic emission analyses, *Geophys. J. Int.,* **177,** 1343–1356.

Wilson, J.E., Chester, J.S. & Chester, F.M., 2003. Microfracture analysis of fault growth and wear processes, Punchbowl Fault, San Andreas system, California, *J. Struct. Geol.,* **25,** 1855–1873.

Wong, T.-F., David, C. & Zhu, W., 1997. The transition from brittle faulting to cataclastic flow in porous sandstones: mechanical deformation, *J. geophys. Res.,* **102,** 3009–3025.

Zienkiewicz, O.C. & Taylor, R.L., 2005. *The Finite Element Method for Solid and Structural Mechanics,* Elsevier Butterworth-Heinemann, Oxford.

Zoback, M.D. *et al*., 1987. New evidence on the state of stress of the San Andreas Fault System, *Science,* **238,** 1105–1111.